J. Fluid Mech. (1996), *vol.* 314, *pp.* 163–189

Axisymmetric pressure-driven flow of rigid pellets through a cylindrical tube lined with a deformable porous wall layer

By E. R. DAMIANO, B. R. DULING, K. LEY AND T. C. SKALAK

Departments of Biomedical Engineering and Physiology, University of Virginia, Charlottesville, VA 22908, USA

(Received 19 May 1995 and in revised form 24 November 1995)

A closed-form analytic solution for the motion of axisymmetric rigid pellets suspended in a Newtonian fluid and driven under a pressure gradient through a rigid impermeable cylindrical tube lined with a porous deformable biphasic wall layer is derived using mixture and lubrication theories. The analysis details the velocity distributions in the lubrication and wall layers as well as the solid-phase displacement field in the wall layer. Expressions for the shear stress and pressure gradient are obtained throughout the lubrication and wall layers. Results are presented in terms of resistance, volume flow, and driving pressure relative to smooth-walled tubes for cases both with and without rigid spheres flowing in the free lumen. The analysis is motivated by its possible relevance to the rheology of blood in the microcirculation wherein the endothelial-cell glycocalyx – a carbohydrate-rich coat of macromolecules consisting of proteoglycans and glycoproteins expressed on the luminal surface of the capillary wall – might exhibit similar behaviour to the wall layer modelled here. Estimates of the permeability of the glycocalyx are taken from experimental data for fibrinogen gels formed *in vitro*. In a tube without pellets lined with a porous wall layer having a thickness which is 15% of the tube radius and having a permeability in the range of fibrinogen gels, approximately a 70% greater pressure drop is required to achieve the same volume flow as would occur in an equivalent smooth-walled tube without a wall layer. If, in the presence of this same wall layer, a rigid spherical pellet is introduced which is 99.5% of the free-lumen radius, the apparent viscosity increases by as much as a factor of four with a concomitant reduction in tube hematocrit of about 10% relative to the corresponding values in an equivalent smooth-walled tube having the same sphere-to-tube diameter ratio without a wall layer.

1. Introduction

The analysis presented here concerns a pressure-driven flow of rigid axisymmetric pellets in a cylindrical tube lined with a uniformly thick porous deformable wall layer. Attention is focused on the effect of the wall layer on the rheological behaviour of the system as a whole and on the interaction between the solid and fluid components of the wall layer. This study is concerned with the axial flow in the tube and the resulting axial deformations which develop in the wall layer. Interest in this problem is motivated by its rheological implications in the smallest blood vessels of the microcirculation, having diameters ranging between 4 and 10 μm. Red cells, which

have a characteristic diameter of 8 μm, experience a large range of deformations in these capillaries. As a result, complex fluid–structure interactions arise between the blood cells, plasma, and vessel walls. Most models of these dynamics assume smooth-walled impermeable tubes as an approximation for the capillary (Skalak & Özkaya 1987; Skalak, Özkaya & Skalak 1989; Secomb 1991, 1995). In fact, the luminal surface of the endothelial cells comprising the capillary wall is lined with a carbohydrate-rich coat or glycocalyx. The endothelial-cell glycocalyx consists of oligosaccharides covalently bound to glycoproteins and proteoglycans composed of long polysaccharide chains covalently bound to a protein core. In addition, plasma proteins such as fibrinogen and albumin can be adsorbed and thus contribute to the solid matrix of macromolecules which comprise the glycocalyx.

The possible relevance of the glycocalyx to microcirculatory function was first considered by Copley and Silberberg (Lahav, Eliezer & Silberberg 1973; Krindel & Silberberg 1979; Copley 1974). Klitzman & Duling (1979) suggested the possible role a glycocalyx might play in accounting for the low volume fractions of red cells which they found in the capillaries of skeletal muscle. Desjardins & Duling (1990) observed a marked increase in the volume fraction of red cells within capillaries after *in vivo* microperfusion of enzymes directed against macromolecules comprising the glycocalyx. Based on their observations, they hypothesized that the glycocalyx could play a role in regulating red-cell volume fraction within microvessels. This hypothesis depends on a number of factors associated with the size and structure of the glycocalyx. Although the material properties are not precisely known, its thickness *in vivo* has been estimated to be on the order of 0.2 to 0.4 μm, or between 10 and 20% of the radius of the smallest capillaries (Gretz 1995). Such a structure could have a significant influence on the resistance to blood flow in the microcirculation as well as on convection in near-wall regions, which in turn could influence material transport across the endothelial-cell membrane. Furthermore, the glycocalyx may serve to attenuate shear stress at the endothelial-cell membrane. It may also play a role in the mechano-transduction of flow and thus be involved in active metabolic processes such as autoregulation.

The rheological behaviour of blood in the circulation is strongly dependent on scale, i.e. the size of its cellular components relative to the diameter of the vessel. Approximately 40% of the blood volume is taken up by deformable red cells with most of the remainder being occupied by blood plasma. The blood plasma itself is Newtonian and incompressible (Chien *et al.* 1966). At high rates of shear, whole blood behaves as a Newtonian fluid having an 'apparent' viscosity (proportional to the ratio of pressure drop to volume flow) which is dependent on hematocrit (volume-fraction of red cells in the blood). However, in tubes having diameters less than 300 μm, the apparent viscosity of blood is seen to decrease as the tube diameter decreases. This trend is attributed mainly to axial concentration which is associated with an inhomogeneous distribution of red cells over the cross-section of the tube. Axial concentration results in a plasma-rich zone in the marginal region of the tube and a cell-rich zone near the core. This configuration favours the regions of highest shear stress near the wall to be borne disproportionately by the relatively low-viscosity plasma. The result is a reduction in the apparent viscosity of the suspension as a whole relative to a uniform distribution of red cells over the vessel cross-section. The reduction in apparent viscosity with decreasing vessel diameter, referred to as the Fåhræus–Lindqvist effect, results in a minimum viscosity value (which depends on hematocrit) near the viscosity of plasma at a critical vessel diameter. Blood flow in still smaller vessels shows a marked increase in apparent viscosity with

decreasing diameter (reviewed by Pries, Neuhaus & Gaehtgens 1992). The reversal of the Fåhræus–Lindqvist effect in the smallest capillaries is a result of the excessive pressures and enhanced viscous drag which develop in the small clearances that are available to the plasma that leaks back around the red cells. This behaviour has been well established for blood flow in glass tubes of varying diameter (Pries *et al.* 1992).

Measurements of blood flow *in vivo* in large-scale microvascular networks together with theoretical network simulations were conducted by Pries *et al.* (1990, 1994). In their analyses, consideration is given to network effects such as heterogeneities which arise owing to phase separation at vessel bifurcations (plasma skimming) as well as local effects associated with the Fåhræus effect (the reduction of tube hematocrit relative to discharge hematocrit with decreasing vessel diameter) and the Fåhræus–Lindqvist effect. Their results were qualitatively similar to those found in glass tubes but dramatically higher apparent viscosities were necessary to account for the predicted resistances arising in vessels below 15 μm. For example, in 10 μm capillaries, the apparent viscosity of blood having a hematocrit of 45% is greater than in glass tubes of the same diameter by approximately a factor of four (Pries *et al.* 1994). This discrepancy was attributed to additional modes of dissipation, not considered in their analysis, associated with local interactions between the red cells and the capillary walls. They pointed to several possibilities which include (i) impeded flow in near-wall regions resulting in increased flow resistance owing to the presence of a glycocalyx, (ii) irregular cross-sectional geometries which may induce transient deformations of passing red cells resulting in increased viscous dissipation in the cell membrane, (iii) vessel bifurcations which result in entrance effects giving rise to enhanced dissipation relative to fully developed flow in straight tubes, and (iv) the presence of less deformable white cells in the microcirculation. In this analysis, we focus on the first explanation by considering a simplified model of the interaction between the endothelial-cell glycocalyx and blood. The macromolecules of the glycocalyx may serve to retard plasma flowing in near-wall regions of microvessels and thereby require increased driving pressure to achieve the same volume flow as would occur in smooth-walled vessels.

To gain insight into the hydroelastic interaction between the endothelial-cell glycocalyx and blood, we consider an idealized system consisting of a rigid impermeable cylindrical tube having a uniform circular cross-sectional area and lined, on its luminal surface, with a uniformly thick porous deformable wall layer. The wall layer is modelled as a biphasic mixture consisting of a linearly elastic solid phase and a linearly viscous fluid phase. A hydrodynamic pressure-driven flow of a Newtonian incompressible fluid is considered for cases both with and without closely fitting rigid axisymmetric pellets flowing in the free lumen (i.e. the 'core region' of the tube that does not contain the wall layer). The pressure, velocity, and displacement fields are found in closed form throughout the lubrication and wall layers.

Wang & Parker (1995) studied the effect of deformable porous layers in a system under hydrostatic pressure in which a heavy rotating rigid sphere falls through a cylindrical tube filled with a quiescent fluid. Their analysis considered a porous layer on both the sphere and tube wall as well as eccentricities of the tube and sphere axes. The similarity with this work lies in the conservation equations governing the wall layer and the use of lubrication theory for the fluid in the gap between the pellet and the wall layer. In their analysis, Wang & Parker argued that when the length scale of velocity variations in the wall layer is small compared with the clearance in the lubrication layer, the effect of the wall layer can be replaced by a slip boundary condition at the interface with the lubrication layer. Their analysis, therefore, does not

detail the velocity distribution in the wall layer. Furthermore, owing to the limitations of two-dimensional lubrication theory which they employed, the lubrication zone did not extend over the entire length of the sphere but was limited to a region on either side of the sphere's equator where the variation in its thickness remained small relative to its length. In the current analysis we employ axisymmetric lubrication theory, extending the range of pellet clearances (see §5.2), and, most importantly, consider a pressure-driven flow of pellets which is directly relevant to the problem of capillary blood flow.

The governing equations for the fluid in the free lumen and in the gap between the surface of the pellet and the wall layer are derived assuming a Stokes flow approximation. Furthermore, when pellets are considered, axisymmetric lubrication theory is assumed to be valid in the gap or lubrication layer between the pellet and the wall layer. Justification for this approximation and the so-called 'zero-drag' condition for neutrally buoyant rigid axisymmetric pellets in cylindrical tubes (see §5.2) has been well established (Wang & Skalak 1969; Tözeren & Skalak 1978; Secomb *et al.* 1986). The governing equations and boundary conditions for the wall layer are derived following methods employed by Mow and coworkers (Mow *et al.* 1980; Lai & Mow 1980; Hou *et al.* 1989, 1990) in their work on cartilage. They employed continuum mechanics of heterogeneous materials described by Truesdell & Toupin (1960) to characterize the multiphasic behaviour of cartilage. An important feature of mixture theory is its ability to account for the interaction between phases manifested by a momentum supply force. The momentum supply is the internal interaction force exerted on one phase by all the other phases in the mixture. It is related to kinematic field variables (such as the deformation and velocity) of each component in the mixture by way of a constitutive relationship that uniquely defines its behaviour. Depending on the constitutive laws which are chosen, very different physics can arise as a result of the interaction between phases from that which could arise from any one of the phases acting separately. The momentum supply force and the boundary conditions for the mixture are the salient features which distinguish this analysis from a simpler viscoelastic model of the wall layer.

In the three sections that follow, the conservation equations and boundary conditions are derived in a generalized vector-invariant form. The model is expressed in axisymmetric cylindrical coordinates in §5 and the cases with and without axisymmetric rigid pellets flowing in the free lumen are considered separately. The analysis is kept general in recognition of its inherently crude approximation to capillary blood flow while bearing in mind its possible applicability to other biological phenomena and/or engineering systems unrelated to microcirculation. Results are given in §6 in terms of driving pressure and volume flow relative to systems without wall layers for the special case of rigid spheres. Finally, §7 discusses the implications of the model in the rheology of the microcirculation.

2. Mixture theory for the biphasic wall layer

The equations governing the biphasic wall layer must satisfy the conservation of mass and momentum. These equations can be obtained for each constituent as well as for the mixture as a whole. It is convenient to express the conservation of mass in terms of a continuity equation for the mixture whereas the momentum equations are best expressed in terms of a system of conservation equations corresponding to each constituent in the mixture. Upon writing the equations of balance, we must specify constitutive equations relating the stresses to the deformation and other kinematical

quantities in the system. The stress tensors for each constituent are formulated in much the same way as they are for a single-phase material without regard to internal interaction forces. Finally, the constitutive relationship for the momentum supply must be specified and may depend on variables associated with both phases. The reduced equations are obtained by combining the constitutive relationships with the conservation equations resulting in a system of differential equations of motion for the mixture.

2.1. *Conservation of mass*

We model the wall layer as a biphasic mixture consisting of a solid phase, having density ρ^s and volume fraction ϕ^s, and a fluid phase, having density ρ^f and volume fraction ϕ^f, subject to the constraint that $\phi^s + \phi^f = 1$. As is commonly assumed for biological tissues, both phases will be taken separately to be intrinsically incompressible such that the material derivative of ρ^α/ϕ^α vanishes (where $\alpha = s, f$). Applying an integral mass balance to the αth constituent occupying a material region of space and using the divergence theorem we obtain (under steady-state conditions)

$$\nabla \cdot (\rho^\alpha \boldsymbol{v}^\alpha) = 0 \tag{2.1}$$

where $\boldsymbol{v}^\alpha$ is the velocity vector of the αth constituent. Imposing the condition of intrinsic phase incompressibility on each of the constituents allows us to express the continuity equation in terms of the volume fraction such that

$$\nabla \cdot (\phi^\alpha \boldsymbol{v}^\alpha) = 0. \tag{2.2}$$

Summing (2.2) over both phases we obtain

$$\nabla \cdot (\phi^s \boldsymbol{v}^s + \phi^f \boldsymbol{v}^f) = 0. \tag{2.3}$$

2.2. *Conservation of momentum*

In the steady state, the conservation of momentum for each constituent is given by

$$\nabla \cdot \boldsymbol{\sigma}^s + \boldsymbol{\pi} = \mathbf{0} \tag{2.4}$$

and

$$\nabla \cdot \boldsymbol{\sigma}^f - \boldsymbol{\pi} = \mathbf{0} \tag{2.5}$$

where $\boldsymbol{\sigma}^\alpha$ is the Cauchy stress tensor for the αth phase and $\boldsymbol{\pi}$ is the momentum supply per unit volume. The momentum supply vector represents an internal interaction force which arises between the two phases in the mixture. In order that the momentum of the total mixture is conserved, the momentum supplied by one constituent must balance the momentum supplied by the other (Truesdell & Toupin 1960).

2.3. *Constitutive equations*

For the purposes of this analysis, we restrict our attention to linear infinitesimal theory. Considering both phases to be isotropic, we model the biphasic wall layer as consisting of a linearly elastic solid, having a shear modulus μ^s and a Lamè coefficient λ^s, and a Newtonian viscous fluid having a dynamic viscosity μ^f. The constitutive relations for the stress tensors of the solid and fluid phases are given respectively by

$$\boldsymbol{\sigma}^s = -\phi^s p \boldsymbol{I} + \lambda^s (\nabla \cdot \boldsymbol{u}^s) \boldsymbol{I} + 2\mu^s \boldsymbol{E}^s \tag{2.6}$$

and

$$\boldsymbol{\sigma}^f = -\phi^f p \boldsymbol{I} - \tfrac{2}{3}\mu^f (\nabla \cdot \boldsymbol{v}^f) \boldsymbol{I} + 2\mu^f \boldsymbol{D}^f \tag{2.7}$$

where p is the pressure and $\boldsymbol{E}^s$ and $\boldsymbol{D}^f$ are the deformation and rate of deformation tensors, respectively. They are defined as follows:

$$\boldsymbol{E}^s = \tfrac{1}{2}(\nabla \boldsymbol{u}^s + (\nabla \boldsymbol{u}^s)^T), \quad \boldsymbol{D}^f = \tfrac{1}{2}(\nabla \boldsymbol{v}^f + (\nabla \boldsymbol{v}^f)^T)$$

where $\boldsymbol{u}^s$ is the displacement vector of the solid phase. In (2.7), we have made use of the Stokes hypothesis and neglected the bulk viscosity of the fluid constituent by taking $\lambda^f = -\frac{2}{3}\mu^f$. The remaining constitutive relation involves the momentum supply. Following Hou *et al.* (1990), we model the force of interaction per unit volume as being related to the velocity difference between phases such that

$$\boldsymbol{\pi} = p\nabla\phi^s + K(\boldsymbol{v}^f - \boldsymbol{v}^s) \tag{2.8}$$

where K is the hydraulic resistivity of the biphasic wall layer. The hydraulic resistivity refers to the pressure drop necessary to achieve a unit volume flow of a specified fluid through a permeable material of unit cross-sectional area and unit thickness (Levick 1987). Lai & Mow (1980) refer to this quantity as the diffusive drag; however, since it characterizes the drag associated with permeation and not with diffusion, we adopt the hydraulic resistivity as a more descriptive term.

2.4. *Reduced equations for a deformable porous wall layer*

Substituting the constitutive relations (2.6), (2.7), and (2.8) into the momentum equations given by (2.4) and (2.5), and making use of the constraint that $\phi^s + \phi^f = 1$, we obtain

$$(\lambda^s + \mu^s)\nabla(\nabla \cdot \boldsymbol{u}^s) + \mu^s\nabla^2\boldsymbol{u}^s = \phi^s\nabla p + K(\boldsymbol{v}^s - \boldsymbol{v}^f) \tag{2.9}$$

and

$$\tfrac{1}{3}\mu^f\nabla(\nabla \cdot \boldsymbol{v}^f) + \mu^f\nabla^2\boldsymbol{v}^f = \phi^f\nabla p + K(\boldsymbol{v}^f - \boldsymbol{v}^s) \tag{2.10}$$

where ∇^2 is the vector Laplacian defined as $\nabla(\nabla\cdot\ ) - \nabla\times(\nabla\times\ )$. Equations (2.9) and (2.10) taken together with the continuity equation given by (2.3) constitute the reduced governing conservation equations given by the field theory.

3. Stokes flow in the free lumen

Modelling the fluid in the free lumen of the tube as Newtonian and incompressible we apply the Stokes equations of motion and the equation of continuity given by

$$\mu^l\nabla^2\boldsymbol{v}^l = \nabla p \tag{3.1}$$

and

$$\nabla \cdot \boldsymbol{v}^l = 0 \tag{3.2}$$

where $\boldsymbol{v}^l$ is the velocity vector of the fluid in the free lumen of the tube and μ^l is fluid's dynamic viscosity. Note that in the absence of pellets, the Stokes equations reduce to a Poiseuille flow in the free lumen of the tube.

4. Boundary conditions

Applying the governing conservation equations of heterogeneous material continua (Truesdell & Toupin 1960) across surfaces of material discontinuity, Hou *et al.* (1989) derived boundary conditions at the interface between multiphasic mixtures and homogeneous materials. As shown by Hou *et al.* (1989), if, at the interfacial surface, Γ, between a fluid and a biphasic mixture, the relative velocity, $\boldsymbol{v}^f - \boldsymbol{v}^s$,

is tangent to Γ, then the volume-weighted sum of the constituent velocities must equal the velocity of the fluid on Γ. This is what they termed the pseudo-no-slip condition. Furthermore, the stress-traction vector, $\boldsymbol{n}\cdot\boldsymbol{\sigma}^{\alpha}$, lying in the interfacial surface associated with the αth phase must equal the volume fraction of that phase times the stress-traction vector of the fluid on Γ. Thus we impose the following boundary conditions at the interfacial surface, Γ^l, separating the biphasic wall layer from the fluid in the free lumen:

$$\phi^s\boldsymbol{v}^s + \phi^f\boldsymbol{v}^f = \boldsymbol{v}^l, \qquad \boldsymbol{x} \in \Gamma^l, \tag{4.1}$$

$$\boldsymbol{n}\cdot\boldsymbol{\sigma}^s = \phi^s\boldsymbol{n}\cdot\boldsymbol{\sigma}^l, \qquad \boldsymbol{x} \in \Gamma^l, \tag{4.2}$$

and

$$\boldsymbol{n}\cdot\boldsymbol{\sigma}^f = \phi^f\boldsymbol{n}\cdot\boldsymbol{\sigma}^l, \qquad \boldsymbol{x} \in \Gamma^l. \tag{4.3}$$

Notice that if we sum (4.2) and (4.3), we obtain $\boldsymbol{n}\cdot(\boldsymbol{\sigma}^s + \boldsymbol{\sigma}^f) = \boldsymbol{n}\cdot\boldsymbol{\sigma}^l$ on $\boldsymbol{x} \in \Gamma^l$ which states that the stress-traction vector of the mixture taken as a whole must equal the stress traction vector of the fluid at the interfacial surface, Γ^l.

At the other interfacial surface, Γ^w, separating the biphasic wall layer from the rigid tube wall, we require that the velocities of the fluid and solid phases are equal to each other and to the velocity of the rigid tube wall. Thus we impose the condition that

$$\boldsymbol{v}^s = \boldsymbol{v}^f = \boldsymbol{v}^w, \qquad \boldsymbol{x} \in \Gamma^w \tag{4.4}$$

where $\boldsymbol{v}^w$ is the velocity of the tube wall. Finally, we must impose the no-slip condition on the fluid at the surface, Γ^p, of the rigid pellet by requiring that

$$\boldsymbol{v}^l = \boldsymbol{v}^p, \qquad \boldsymbol{x} \in \Gamma^p \tag{4.5}$$

where $\boldsymbol{v}^p$ is the velocity of the pellet.

5. Problem for the deformable porous wall layer with an axisymmetric axial flow

In the problem we will consider for the remainder of this analysis, we restrict our attention to a one-component axisymmetric axial flow field. This approximation is reasonable for circular-cylindrical tubes having a uniform cross-sectional radius, R, and a uniformly thick deformable wall layer. For this geometry we first consider the problem of a simple Newtonian fluid, free of pellets, flowing in the free lumen. This is similar to the classical Beavers–Joseph problem (Beavers & Joseph 1967; Hou *et al.* 1989) except we will be using axisymmetric cylindrical coordinates, r and z. Next we consider the flow of rigid axisymmetric pellets which nearly fill the free lumen of the tube. For reasons discussed later, relating to the limitations of the infinitesimal theory used here, we will only consider pellets with diameters strictly less than the diameter, a, of the free lumen.

Figure 1 shows a schematic of a rigid cylindrical tube lined with a deformable porous wall layer. The tube contains a Newtonian fluid driven by an imposed pressure gradient. If pellets are flowing in the free lumen, the pressure gradient will vary through the lubrication and wall layers as a function of z, whereas sufficiently far away from pellets or in pellet-free flow, the pressure gradient remains constant. Thus, for a uni-directional axisymmetric axial flow the non-vanishing steady-state field components are the velocities, $v_z^f = v_z^f(r,z)$ and $v_z^l = v_z^l(r,z)$, the deformation, $u_z^s = u_z^s(r,z)$, and the pressure, $p = p(z)$.

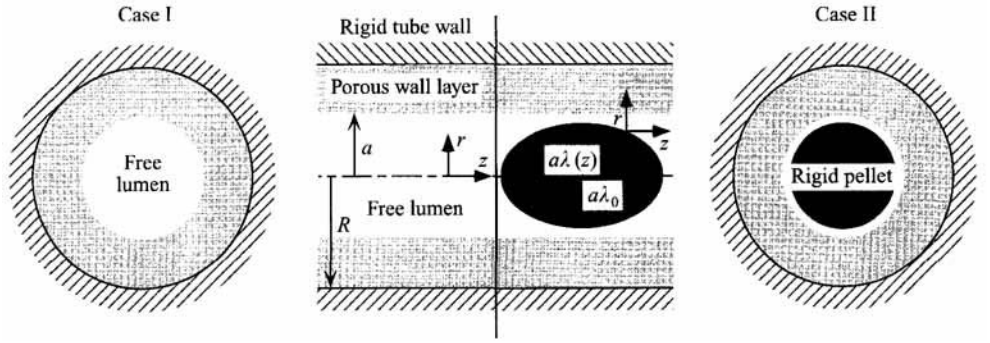

FIGURE 1. Schematic of an impermeable rigid cylindrical tube lined with a deformable porous wall layer. The two cases considered include a Newtonian fluid flowing in the free lumen driven by an imposed pressure gradient (case I) and a pressure-driven flow of rigid axisymmetric pellets suspended in a Newtonian fluid (case II). Only pellets with diameters strictly less than the diameter of the free lumen are considered. The free-lumen radius a and the tube radius R characterize the dimensionless wall-layer thickness, $1 - a/R = 1 - \alpha$. The maximum pellet radius is given by $a\lambda_0$ where $\lambda_0 < 1$ and the curve describing the surface of the pellet is defined parametrically by the function $a\lambda(z)$ where $0 < \lambda(z) \leqslant \lambda_0$. For axisymmetric flow, r and z are cylindrical coordinates which are defined on $0 \leqslant r \leqslant R$ and $-\infty \leqslant z \leqslant \infty$ for case I and $a\lambda(z) \leqslant r \leqslant R$ and $-a\lambda_0 < z < a\lambda_0$ for case II.

5.1. *Case I: Newtonian fluid flowing in tube – Poiseuille flow in free lumen*

For a Newtonian fluid flowing in the tube, the pressure gradient is constant and the field equations for the biphasic wall layer, given by (2.9), (2.10), and (2.3), thus reduce to the following scalar form:

$$\frac{\mu^s}{r}\frac{\partial}{\partial r}\left(r\frac{\partial u_z^s}{\partial r}\right) = \phi^s\frac{\partial p}{\partial z} - Kv_z^f, \qquad a \leqslant r \leqslant R, \tag{5.1}$$

$$\frac{\mu^f}{r}\frac{\partial}{\partial r}\left(r\frac{\partial v_z^f}{\partial r}\right) = \phi^f\frac{\partial p}{\partial z} + Kv_z^f, \qquad a \leqslant r \leqslant R, \tag{5.2}$$

and

$$\frac{\partial u_z^s}{\partial z} = \frac{\partial v_z^f}{\partial z} = 0, \qquad a \leqslant r \leqslant R \tag{5.3}$$

where we have made the approximation $v_z^s \approx \partial u_z^s/\partial t = 0$ which is consistent with the infinitesimal-strain theory we have employed. Notice that for constant volume fractions, the momentum equation for the fluid phase in the wall layer, given by (5.2), is uncoupled from that of the solid phase. Further notice that if the drag of interaction between phases in the wall layer is large compared to viscous effects, and the Laplacian term on the left-hand side of (5.2) is neglected, the mixture theory reduces to Darcy's law in which the fluid velocity in the wall layer is constant and proportional to the pressure gradient. The fluid in the free lumen is governed by Poiseuille's equation and is given by

$$\frac{\mu^l}{r}\frac{\partial}{\partial r}\left(r\frac{\partial v_z^l}{\partial r}\right) = \frac{\partial p}{\partial z}, \qquad 0 \leqslant r \leqslant a, \tag{5.4}$$

with the continuity equation given by

$$\frac{\partial v_z^l}{\partial z} = 0, \qquad 0 \leqslant r \leqslant a. \tag{5.5}$$

The boundary conditions involving the stress tractions at the interface, Γ^l, between the free lumen and the porous wall layer, given by (4.2) and (4.3), reduce to

$$\left.\frac{\partial u_z^s}{\partial r}\right|_{r=a} = \left.\frac{\phi^s \mu^l}{\mu^s}\frac{\partial v_z^l}{\partial r}\right|_{r=a} \quad \text{and} \quad \left.\frac{\partial v_z^f}{\partial r}\right|_{r=a} = \left.\frac{\phi^f \mu^l}{\mu^f}\frac{\partial v_z^l}{\partial r}\right|_{r=a} \tag{5.6a,b}$$

while the pseudo-no-slip condition on Γ^l, given by (4.1), reduces to

$$v_z^l(a) = \phi^f v_z^f(a). \tag{5.7}$$

The remaining boundary condition, given by (4.4), is the no-slip condition at the interface, Γ^w, between the porous wall layer and the rigid tube wall. It reduces to

$$u_z^s(R) = 0 \quad \text{and} \quad v_z^f(R) = 0. \tag{5.8a,b}$$

Non-dimensionalizing, we define $\tilde{r} = r/R$, and the dimensionless displacement and velocities as

$$\tilde{u}^s(\tilde{r}) = \frac{u_z^s(r)\phi^s\mu^s}{R^2(-\mathrm{d}p/\mathrm{d}z)}, \quad \tilde{v}^f(\tilde{r}) = \frac{v_z^f(r)\phi^f\mu^l}{R^2(-\mathrm{d}p/\mathrm{d}z)}, \quad \tilde{v}^l(\tilde{r}) = \frac{v_z^l(r)\phi^f\mu^l}{R^2(-\mathrm{d}p/\mathrm{d}z)}. \tag{5.9}$$

We further introduce the following dimensionless quantities

$$\alpha = a/R, \quad \delta = \left(\frac{\mu^f}{R^2K}\right)^{1/2}, \quad \eta = \frac{(\phi^f)^2\mu^l}{\mu^f} \tag{5.10}$$

where δ represents the ratio of viscous drag forces to hydraulic resistance forces in the wall layer and η represents the weighted viscosity ratio of the fluid in the free lumen to the fluid in the wall layer. The solutions to (5.1), (5.2), and (5.4) subject to the boundary conditions above are

$$\frac{\tilde{u}^s(\tilde{r})}{\phi^s} = \tfrac{1}{4}(1-\tilde{r}^2) - \frac{\phi^f}{\eta}\tilde{v}^f(\tilde{r}), \quad \alpha \leqslant \tilde{r} \leqslant 1, \tag{5.11}$$

$$\tilde{v}^f(\tilde{r}) = -\eta\,\delta^2\left\{\left(\frac{\alpha}{2\delta} + \frac{K_1(\alpha/\delta)}{K_0(1/\delta)}\right)\frac{I_0(\tilde{r}/\delta) - \beta K_0(\tilde{r}/\delta)}{I_1(\alpha/\delta) + \beta K_1(\alpha/\delta)} + \frac{K_0(\tilde{r}/\delta)}{K_0(1/\delta)} - 1\right\}, \quad \alpha \leqslant \tilde{r} \leqslant 1, \tag{5.12}$$

and

$$\frac{\tilde{v}^l(\tilde{r})}{\phi^f} = -\eta\,\delta^2\left\{\left(\frac{\alpha}{2\delta} + \frac{K_1(\alpha/\delta)}{K_0(1/\delta)}\right)\frac{I_0(\alpha/\delta) - \beta K_0(\alpha/\delta)}{I_1(\alpha/\delta) + \beta K_1(\alpha/\delta)} + \frac{K_0(\alpha/\delta)}{K_0(1/\delta)} - 1\right\} + \tfrac{1}{4}(\alpha^2 - \tilde{r}^2), \quad 0 \leqslant \tilde{r} \leqslant \alpha, \tag{5.13}$$

where $\beta = I_0(1/\delta)/K_0(1/\delta)$. Here, I_0 and K_0 are, respectively, the modified zeroth-order Bessel functions of the first and second kind and I_1 and K_1 are the modified first-order Bessel functions of the first and second kind.

5.2. *Case II: Rigid pellets flowing in free lumen – axisymmetric lubrication theory*

Some of the earliest attempts to describe the flow of deformable red cells through capillaries using lubrication theory were made by Lighthill (1968) and Barnard, Lopez & Hellums (1968). Lighthill applied two-dimensional lubrication theory to elastic compressible pellets forced through elastic distensible tubes filled with a pressure-driven Newtonian incompressible fluid. Fitz-gerald (1969) extended Lighthill's work and considered both the axisymmetric and asymmetric cases as well as the effect of

a porous capillary wall. Secomb *et al.* (1986) pointed out that lubrication theory yielded very accurate results for rigid spheres when compared with exact solutions of the Stokes equations obtained in the form of series expansions by Wang & Skalak (1969). These closed-form series solutions provided the radial and axial velocity components of a creeping axisymmetric viscous flow containing a line of spherical particles. The pressure drop across the sphere predicted by axisymmetric lubrication theory was shown by Secomb *et al.* (1986) to agree closely with the exact solution of Wang & Skalak (1969) even for spheres with diameters as small as 60% that of the tube diameter. They further argued that lubrication theory should yield still better approximations for more elongated pellets since the ratio of the thickness of the lubrication layer to its length would then be smaller than for spheres. By comparison, they showed that two-dimensional lubrication theory yields results which are accurate only for spheres with diameters greater than 90% of the tube diameter.

The introduction of a pellet has the important implication that the pressure and velocity become functions of the axial coordinate, z. Although we admit z-dependence into our velocity field, we still invoke the approximation from lubrication theory that derivatives with respect to z are small compared with their corresponding derivatives in the r-direction, provided the lubricating layer is sufficiently thin compared with its length. As in the case without pellets, therefore, we still make the approximation that the Laplacian in (2.9), (2.10), and (3.1) depends only on r and is independent of z in the axisymmetric case. This approximation is reasonable even near the leading and trailing edges of the pellet where the lubrication layer may become quite large. This is because the pressure in these regions is typically small by comparison to values it assumes in regions where the gap is thinnest. Admitting z-dependence into the pressure gradient and velocity fields adds considerable algebraic complexity to the problem; however the closed-form analytic solution still remains tractable.

We may now formulate the problem of a pressure-driven flow of rigid pellets in the free lumen. In keeping with our assumption of small deformations of the solid phase in the wall layer, we consider only those pellets with diameters strictly less than the diameter of the free lumen. Thus, for pellets defined parametrically by the function $a\lambda(z)$, we require $0 < \lambda(z) < 1$ (in the case of a sphere, $a\lambda(z) = \lambda_0(a^2 - z^2/\lambda_0^2)^{1/2}$, where λ_0 is the maximum sphere radius relative to the free-lumen radius, a). The boundary-value problem just considered is applicable to the problem with pellets if we invoke the additional boundary condition, given by (4.5), which states that the fluid velocity on the surface of the pellet must equal the pellet velocity, and replace the continuity equations, given by (5.3) and (5.5), with the integrated form of the continuity equation with respect to the cross-section of the tube. Thus the boundary-value problem with rigid pellets is defined by the momentum equations given by (5.1), (5.2), and (5.4) (where the radial coordinate in (5.4) is defined when $a\lambda(z) \leqslant r \leqslant a$). The boundary conditions are given by (5.6)–(5.8), with the additional no-slip condition on the pellet surface given by

$$v_z^l(a\lambda(z), z) = v_0, \tag{5.14}$$

and the continuity equation is given by

$$Rq_0 = \tfrac{1}{2}v_0(a\lambda)^2 + \int_{a\lambda}^{a} v_z^l(r,z)\, r\, \mathrm{d}r + \phi^f \int_a^R v_z^f(r,z)\, r\, \mathrm{d}r. \tag{5.15}$$

Here we define v_0 as the velocity of the pellet and q_0 as the total volume flow per

unit tube circumference at an arbitrary cross-section of the tube. The first term on the right-hand side above represents the volume flow of the solid pellet as a function of z. The second and third terms correspond to the volume flow of fluid in the lubrication and wall layers, respectively. Since this fluid is assumed incompressible, the total volume flow, q_0, which remains an unknown quantity, is necessarily constant and therefore independent of z.

The statement of the boundary condition on the pellet given by (5.14) is consistent with choosing a frame of reference attached to the tube wall. Most analyses of capillary blood flow attach the reference frame to the pellet (Lighthill 1968; Tözeren & Skalak 1978; Secomb *et al.* 1986) resulting in a truly steady-state problem. In such a reference configuration the volume of fluid that leaks back around the pellet is constant at every cross-section whereas in the configuration we have chosen, the leakback depends on z and is given by the sum of the second two terms on the right-hand side of (5.15), representing the difference between the total volume flow, Rq_0, and the local volume flow of the sphere, $\frac{1}{2}v_0(a\lambda)^2$. Attaching a frame of reference to the tube wall results in a simpler constitutive relationship for the wall layer.

The integration constant, q_0, arising from the continuity equation given by (5.15) may be determined by applying a force balance to a control volume over a section of the tube containing the sphere. For neutrally buoyant pellets, we impose the so-called 'zero-drag' condition (Lighthill 1968; Tözeren & Skalak 1978). This may be stated as follows: from a control-volume analysis on a steady Stokes flow, and in the light of the fact that a neutrally buoyant pellet can exert no net external force on the control volume, we impose the condition of zero drag on the pellet by requiring that, in the lubrication and wall layers bounded by the leading and trailing edges of the pellet, the total pressure drop across the pellet must exactly balance the resultant of the total shear stress acting on the tube wall. This condition is given by

$$2\pi R \int_{z_1}^{z_2} \left(\frac{R}{2} \frac{\mathrm{d}p}{\mathrm{d}z} - \tau_w \right) \mathrm{d}z = 0 \tag{5.16}$$

where z_2 and z_1 are the coordinates corresponding to the leading and trailing edges of the pellet, respectively, and $\tau_w = (\tau_{rz})|_{r=R}$ is the shear stress on Γ^w, the interface between the biphasic wall layer and the rigid tube wall. In general, the shear stress, τ_{rz}, in the lubrication and wall layers is given by

$$\tau_{rz}(r,z) = \begin{cases} \mu^l \dfrac{\partial v_z^l}{\partial r}, & \text{if } a\lambda \leqslant r \leqslant a \\ \\ \mu^s \dfrac{\partial u_z^s}{\partial r} + \mu^f \dfrac{\partial v_z^f}{\partial r}, & \text{if } a \leqslant r \leqslant R. \end{cases} \tag{5.17}$$

Notice that the shear stress in the wall layer, corresponding to the second expression above, represents the total shear stress and is therefore the sum of the stresses in both phases of the mixture. This is consistent with the reasoning which led to the formulation of the boundary conditions given by (4.2) and (4.3).

With the foregoing statement of the problem just defined, we may write the solution to the fluid velocity in the wall and lubrication layers, governed by (5.2) and (5.4), respectively, as

$$v_z^f(\tilde{r},z) = A(z)\left(I_0(\tilde{r}/\delta) - \beta K_0(\tilde{r}/\delta)\right) + \phi^f \delta^2 \left(\frac{K_0(\tilde{r}/\delta)}{K_0(1/\delta)} - 1 \right) \frac{R^2}{\mu^f} \frac{\mathrm{d}p}{\mathrm{d}z}, \quad \alpha \leqslant \tilde{r} \leqslant 1 \tag{5.18}$$

and

$$v_z^l(\tilde{r},z) = \frac{(\phi^f)^2}{\eta}\frac{R^2}{4\mu^f}\frac{\mathrm{d}p}{\mathrm{d}z}\tilde{r}^2 + B(z)\ln\tilde{r} + C(z), \quad \alpha\lambda \leqslant \tilde{r} \leqslant \alpha \tag{5.19}$$

where $A(z)$, $B(z)$ and $C(z)$ are arbitrary functions of integration, and the pressure, p, is as yet an unknown function of z. In addition to the pressure, the other fundamental mathematical distinction between the problem with pellets and the problem without is the inclusion of the logarithmic term in (5.19) which satisfies (5.4). This term was not admissible in the solution to the pellet-free problem owing to the logarithmic singularity which arises as r approaches zero. Since r does not vanish on the surface of the pellet (except at the two points corresponding to the leading and trailing edges of the pellet), the logarithmic term remains bounded in the lubrication and wall layers and must appear, in addition to the quadratic term, as the other linearly independent solution.

The solution to the solid-phase displacement of the wall layer, $u_z^s(\tilde{r},z)$, is a combination of the solutions (5.18) and (5.19) which must be made to satisfy the differential equation and boundary conditions pertaining to u_z^s. As with v_z^l, the solution form for u_z^s is similar to the solution without pellets, given by (5.11), with the addition of the logarithmic term. This term is admitted since $\ln\tilde{r}$ appears in (5.19), is a solution to the differential equation given by (5.1), and vanishes at the boundary $\tilde{r} = 1$, thus satisfying the no-slip boundary condition given by (5.8*a*). Imposing the remaining boundary condition on u_z^s given by (5.6*a*), we obtain the solution for the solid-phase displacement of the wall layer given by

$$u_z^s(\tilde{r},z) = -\frac{R^2}{4\mu^s}\frac{\mathrm{d}p}{\mathrm{d}z}(1-\tilde{r}^2) + \frac{\mu^f}{\mu^s}\left(\frac{\eta}{(\phi^f)^2}B(z)\ln\tilde{r} - v_z^f(\tilde{r},z)\right), \quad \alpha \leqslant \tilde{r} \leqslant 1. \tag{5.20}$$

The expression given by (5.18) for the fluid-phase velocity in the wall layer was made to automatically satisfy the no-slip condition given by (5.8*b*) when $\tilde{r} = 1$. Imposing the three remaining conditions, i.e. the two pertaining to the fluid phase at the interface between the wall and lubricating layers, given by (5.6*b*) and (5.7), and the no-slip condition on the pellet surface, given by (5.14), we obtain the following expressions for the arbitrary functions of integration in terms of the unknown pressure gradient:

$$A(z) = \frac{v_0}{X_1} + \frac{X_2}{X_1}\frac{R^2}{\mu^f}\frac{\mathrm{d}p}{\mathrm{d}z}, \tag{5.21}$$

$$B(z) = \frac{X_3}{X_1}v_0 + \left(\frac{X_2X_3}{X_1} - X_4\right)\frac{R^2}{\mu^f}\frac{\mathrm{d}p}{\mathrm{d}z}, \tag{5.22}$$

$$C(z) = \left(\frac{X_5}{X_1} - \frac{\ln\alpha}{\ln\lambda}\right)v_0 + \left(\frac{X_2X_5}{X_1} + X_6\right)\frac{R^2}{\mu^f}\frac{\mathrm{d}p}{\mathrm{d}z} \tag{5.23}$$

where

$$X_1 = \frac{\alpha\phi^f}{\delta\eta}\ln\lambda\left(I_1(\alpha/\delta) + \beta K_1(\alpha/\delta)\right) + \phi^f\left(I_0(\alpha/\delta) - \beta K_0(\alpha/\delta)\right),$$

$$X_2 = (\phi^f)^2\delta^2\left(1 - \frac{K_0(\alpha/\delta)}{K_0(1/\delta)}\right) + \frac{\alpha^2(\phi^f)^2}{\eta}\left(\tfrac{1}{2}\ln\lambda + \tfrac{1}{4}(1-\lambda^2) + \frac{\delta\ln\lambda}{\alpha}\frac{K_1(\alpha/\delta)}{K_0(1/\delta)}\right),$$

$$X_3 = \frac{\alpha\phi^f}{\delta\eta}\left(I_1(\alpha/\delta) + \beta K_1(\alpha/\delta)\right),$$

$$X_4 = \frac{\alpha(\phi^f)^2}{\eta}\left(\frac{\alpha}{2} + \delta\frac{K_1(\alpha/\delta)}{K_0(1/\delta)}\right),$$

$$X_5 = \phi^f\frac{\ln(\alpha\lambda)}{\ln\lambda}\left(I_0(\alpha/\delta) - \beta K_0(\alpha/\delta)\right),$$

$$X_6 = (\phi^f)^2\delta^2\frac{\ln(\alpha\lambda)}{\ln\lambda}\left(\frac{K_0(\alpha/\delta)}{K_0(1/\delta)} - 1\right) - \frac{\alpha^2(\phi^f)^2}{4\eta}\left(1 + \frac{\ln\alpha}{\ln\lambda}(1-\lambda^2)\right).$$

Imposing the integral form of the continuity equation, we substitute (5.18) and (5.19) into (5.15). Collecting quantities in terms of the pressure gradient we obtain the following Reynolds equation for rigid pellets flowing through a rigid tube lined with a porous wall layer:

$$\frac{R^2}{\mu^f}\frac{\mathrm{d}p}{\mathrm{d}z} = v_0\left\{\frac{q_0}{Rv_0} - \tfrac{1}{2}(\alpha\lambda)^2 - \tfrac{1}{2}\alpha^2(1-\lambda^2)\left[\frac{X_3}{X_1}\left(\ln\alpha - \tfrac{1}{2} - \frac{\lambda^2\ln\lambda}{1-\lambda^2}\right) + \frac{X_5}{X_1} - \frac{\ln\alpha}{\ln\lambda}\right]\right.$$
$$\left. - \frac{\phi^f}{X_1}\langle 1, I_0 - \beta K_0\rangle\right\} \Bigg/ \left\{\phi^f\frac{X_2}{X_1}\langle 1, I_0 - \beta K_0\rangle + (\phi^f)^2\delta^2\left(\frac{\langle 1, K_0\rangle}{K_0(1/\delta)} - \tfrac{1}{2}(1-\alpha^2)\right)\right.$$
$$+\tfrac{1}{2}\alpha^2(1-\lambda^2)\left[\frac{\alpha^2(\phi^f)^2}{8\eta}(1+\lambda^2) + \left(\frac{X_2X_3}{X_1} - X_4\right)\left(\ln\alpha - \tfrac{1}{2} - \frac{\lambda^2\ln\lambda}{1-\lambda^2}\right)\right.$$
$$\left.\left. + \frac{X_2X_5}{X_1} + X_6\right]\right\} \tag{5.24}$$

where the domain of the inner products appearing in (5.24) is defined with respect to the cross-sectional area of the wall layer such that

$$\langle 1, K_0\rangle = \int_\alpha^1 K_0(\tilde{r}/\delta)\,\tilde{r}\,\mathrm{d}\tilde{r}, \qquad \langle 1, I_0 - \beta K_0\rangle = \int_\alpha^1 \left(I_0(\tilde{r}/\delta) - \beta K_0(\tilde{r}/\delta)\right)\tilde{r}\,\mathrm{d}\tilde{r}. \tag{5.25}$$

Thus, for a specific axisymmetric pellet shape, $\lambda(z)$, the Reynolds equation, given by (5.24), is known to within an arbitrary constant, q_0. In order to determine this constant, we apply the zero-drag condition given by (5.16). First we must determine the shear stress acting at the interface between the biphasic wall layer and the rigid tube wall. From (5.17), the shear stress acting in the lubrication and wall layers is given by

$$\tau_{rz}(\tilde{r}, z) = \frac{R}{2}\frac{\mathrm{d}p}{\mathrm{d}z}\tilde{r} + \frac{\mu^l}{R}\frac{B(z)}{\tilde{r}}, \qquad \alpha\lambda \leqslant \tilde{r} \leqslant 1. \tag{5.26}$$

The shear stress at the wall, τ_w, is therefore given by

$$\tau_w(z) = \frac{R}{2}\frac{\mathrm{d}p}{\mathrm{d}z} + \frac{\mu^l}{R}B(z). \tag{5.27}$$

In the light of this relationship, application of the zero-drag condition given by (5.16) provides an implicit expression for the total volume flow, q_0, given by

$$\int_{z_1}^{z_2} B(z)\mathrm{d}z = 0. \tag{5.28}$$

Recall that $B(z)$ depends on the pressure gradient, $\mathrm{d}p/\mathrm{d}z$. For the sake of brevity, we define the functions $f(z)$ and $g(z)$ such that the right-hand side of (5.24) may be expressed as $v_0\{Q_0 - f(z)\}/g(z)$, where $Q_0 = q_0/Rv_0$ is the dimensionless volume flow. Substituting $B(z)$, given by (5.22), into the above expression for the zero-drag condition, we obtain the following equation for the dimensionless volume flow,

Q_0, determined explicitly in terms of the shape of the axisymmetric rigid pellet, $\lambda(z)$:

$$Q_0 = \frac{\displaystyle\int_{z_1}^{z_2} \left\{ \left(\frac{X_2 X_3}{X_1} - X_4 \right) \frac{f(z)}{g(z)} - \frac{X_3}{X_1} \frac{(\phi^f)^2}{\eta} \right\} \mathrm{d}z}{\displaystyle\int_{z_1}^{z_2} \left(\frac{X_2 X_3}{X_1} - X_4 \right) \frac{\mathrm{d}z}{g(z)}}. \tag{5.29}$$

Specification of an axisymmetric pellet shape (having a maximum radius strictly less than the radius of the free lumen) provides the dimensionless volume flow, Q_0, given by (5.29), which in turn provides the necessary constant that renders the pressure, velocity, and deformation fields, given by (5.18), (5.19), (5.20), and (5.24), as the unique analytic closed-form solution to the boundary-value problem put forth.

6. Results with and without close-fitting rigid spheres

Figure 2 shows the dimensionless displacement and volume-weighted velocity profiles, $\tilde{u}^s$, $\tilde{v}^f$, and $\tilde{v}^l/\phi^f$ given by (5.11)–(5.13) for flow of a Newtonian fluid through a tube lined with a porous deformable wall layer as a function of $\tilde{r}$ for two values of the dimensionless wall-layer thickness ($1 - \alpha = 0.5$ on the left and 0.2 on the right) and four values of the reciprocal dimensionless wall drag, δ^2. The velocity components are normalized relative to the centreline velocity of the Poiseuille distribution that arises under the same pressure drop in the absence of a wall layer. The curves correspond to a weighted viscosity ratio, η, of 0.98, and a fluid volume fraction, ϕ^f, of about 0.99, implying a uniform viscosity throughout the tube ($\mu^l = \mu^f$). In the velocity profiles of figure 2(*a*,*b*), we see that as the drag associated with permeation increases relative to the viscous drag (i.e. as δ^2 tends toward zero), the velocity profile in the wall layer tends to become more uniform with a boundary layer or transitional region developing at the interface between the wall layer and the fluid in the free lumen. This behaviour could be anticipated by examination of the equation modelling the fluid phase in the wall layer given by (5.2). As the hydraulic resistivity term becomes large and overwhelms the effect of the viscous dissipation term, the model governing the fluid phase approaches Darcy's law, which predicts a constant velocity field proportional to the uniform pressure gradient. Alternatively, as the viscous drag in the wall layer becomes large relative to the drag associated with permeation (i.e. as δ^2 becomes large), the velocity profiles in (*a*) and (*b*) approach a Poiseuille distribution. As we see from (5.2), when the viscous dissipation term becomes large relative to the hydraulic resistivity term, Poiseuille's equation is recovered in which the pressure gradient is scaled by the porosity, ϕ^f. Thus we see a parabolic velocity profile emerging in the wall layer as δ^2 becomes large. The dimensionless velocity profile for a Poiseuille flow with no wall layer corresponds to the parabola shown by the dotted curve in (*a*) and (*b*).

Figures 2(*c*) and 2(*d*) show the dimensionless displacement profiles, in the absence of pellets, of the solid phase in the wall layer for four values of δ^2. As δ^2 becomes small, the hydraulic resistivity begins to dominate over viscous dissipation and the deformation of the solid phase in the wall layer increases. Since the permeability (hydraulic conductivity) is inversely proportional to the hydraulic resistivity, it decreases with decreasing δ^2. For a constant pressure gradient, as the permeability decreases, the fluid phase becomes more difficult to force through the solid matrix, resulting in enhanced deformation of the solid phase. Alternatively, one could argue that since the shear stress in the fluid phase decreases with decreasing δ^2, as evidenced by the corresponding velocity gradients in (*a*) and (*b*), the stress must be borne to a greater

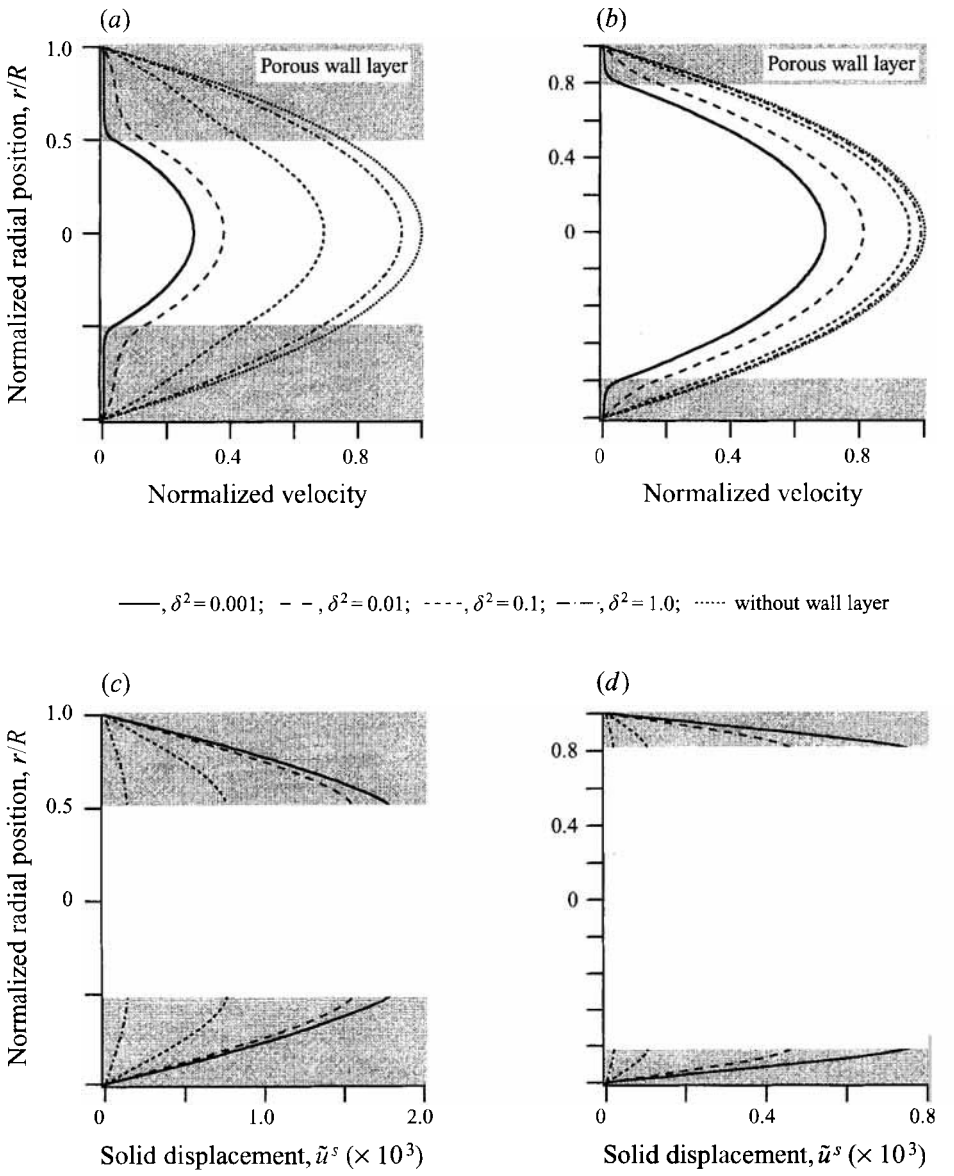

FIGURE 2. Normalized volume-weighted fluid velocity profiles in the wall layer (shaded region) and free lumen, (*a*) and (*b*), and dimensionless solid-phase displacement profiles in the wall layer, (*c*) and (*d*), for a Newtonian fluid flowing in the tube, corresponding to four values of the reciprocal dimensionless wall drag, δ^2. The dimensionless wall-layer thickness, $1-\alpha$, is 50% in (*a*) and (*c*) and 20% in (*b*) and (*d*). The Poiseuille profile which would arise in the absence of a wall layer is shown by the dotted parabola in (*a*) and (*b*). The velocity profiles are normalized relative to the centreline velocity of the Poiseuille distribution that arises under the same pressure drop without a wall layer. The solid-phase displacement in the wall layer is non-dimensionalized with respect to $R^2(-\mathrm{d}p/\mathrm{d}z)/\phi^s\mu^s$. The porosity, ϕ^f, is 0.99 and the viscosity is taken to be uniform throughout the free lumen and wall layer (i.e. $\eta = 0.98$).

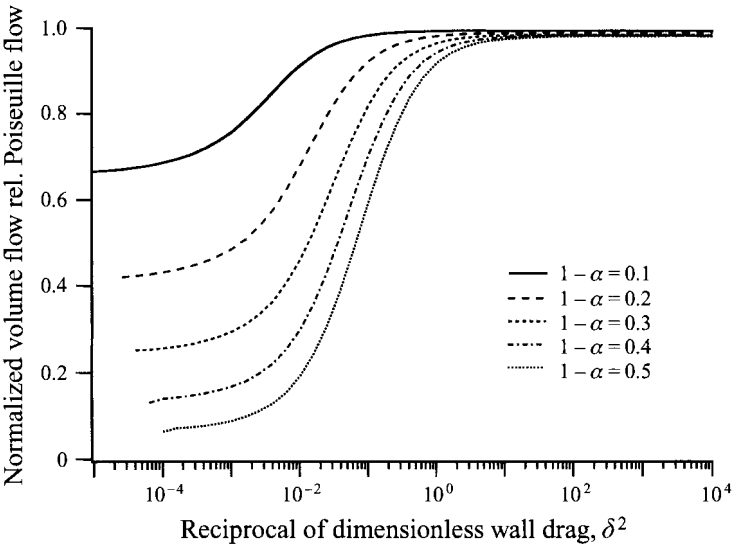

FIGURE 3. Volumetric flow rate in a tube lined with a porous wall layer without pellets, relative to a Poiseuille flow in a rigid tube of radius R, is shown as a function of the reciprocal dimensionless wall drag, δ^2, for five dimensionless wall-layer thicknesses ($1-\alpha = 0.1$, 0.2, 0.3, 0.4 and 0.5). As the permeability tends toward zero, the flow in the wall layer also approaches zero. In the limit of zero permeability, the entire volume flow is constrained to a Poiseuille flow in the free-lumen region of the tube's cross-section. According to Poiseuille's law, the five curves asymptote to the fourth power of the dimensionless free-lumen radius, α. All parameters as in figure 2.

extent by the solid phase in the mixture. Thus, the deformation and deformation gradients of the solid phase increase as δ^2 tends toward zero.

Since the porous wall layer lines the tube wall, it occupies the outer-most regions of the cross-sectional area, and even a thin layer can retard a significant volume of fluid, provided the hydraulic resistivity is sufficiently large. Figure 3 shows the volumetric flow rate plotted as a function of δ^2, the reciprocal dimensionless wall drag, for five different values of the dimensionless wall-layer thickness, $1-\alpha$. As the dimensionless wall drag, $1/\delta^2$, becomes large (i.e. as δ^2 tends toward zero), the porous wall approaches a rigid wall, decreasing the effective cross-sectional radius by the thickness of the wall layer. Since the volumetric flow rate for a Poiseuille distribution is proportional to the fourth power of the tube radius, we anticipate a lower bound on the volumetric flow rate of $\alpha^4 = a^4/R^4$ which corresponds to the lower asymptotes associated with the curves in figure 3. In the other limit, as the drag due to permeation becomes small relative to the viscous drag (i.e. as δ^2 becomes large), we see that, for a given porosity, the dimensionless volumetric flow rates asymptote to values which depend upon the thickness of the wall layer. The dependence of these upper asymptotes on wall-layer thickness and porosity results from the fact that the solid phase occupies volume in the wall layer and thus reduces the cross-sectional area of the tube that is available to fluid flow relative to a tube of equivalent diameter without a wall layer. For a given porosity, this volume exclusion increases with increasing wall-layer thickness resulting in a decreased upper asymptote. Alternatively, for a given wall-layer thickness, these asymptotes increase with increasing wall-layer porosity. In the limit as the solid volume fraction approaches zero, the upper asymptotes in figure 3 would all coincide with unity, independent of the wall-layer thickness just as they would in the limit of a vanishing wall-layer thickness for any given value of

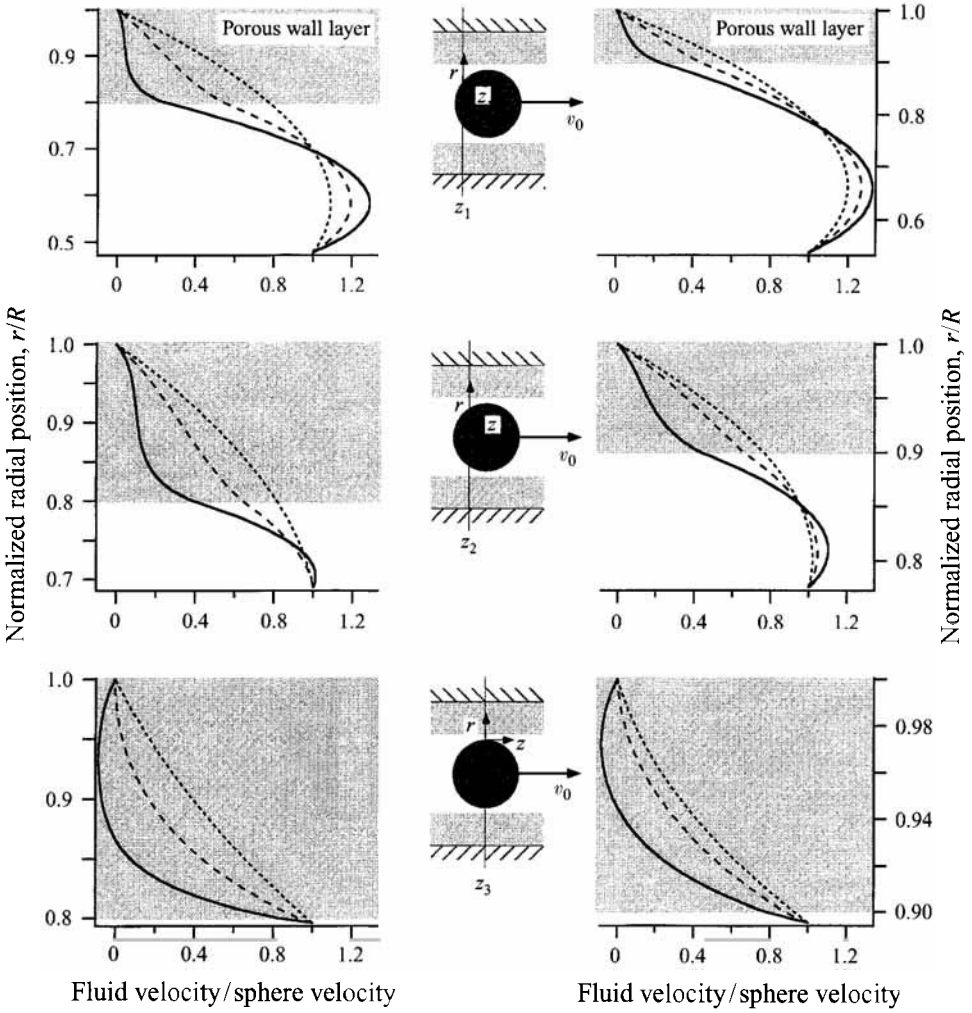

FIGURE 4. Normalized volume-weighted fluid velocity profiles in the wall layer (shaded region) and lubrication layer which arise in the presence of a rigid sphere flowing in the free lumen. The velocity profiles, normalized with respect to the sphere velocity, are shown at three axial locations in z and for two dimensionless wall-layer thicknesses (20% on the left and 10% on the right). The solid (——) and dashed (– – –) curves correspond to a reciprocal dimensionless wall drag of $\delta^2 = 0.001$ and 0.01, respectively. The dotted curves (- - - - -) correspond to profiles that would occur in the absence of a wall layer. The illustrations in the centre of the figure show at what station on the sphere, z_1, z_2, or z_3, the velocity profiles are being evaluated. The sphere moves to the right at velocity v_0. For both wall layers considered, the sphere radius is 99.5% of the free-lumen radius ($\lambda_0 = 0.995$). Other parameters as in figure 2. Notice that the ordinate scales differ in each panel.

porosity. Owing to the high porosity associated with the curves in figure 3, the upper asymptotes all lie close to a normalized volume flow of 1.

Figure 4 shows the profiles of the volume-weighted normalized velocities, $\phi^f v_z^f / v_0$, in the wall layer, given by (5.18), and v_z^l / v_0 in the lubrication layer, given by (5.19), which develop in the presence of a rigid sphere having a radius which is 99.5% of the free-lumen radius. The three panels on the left correspond to a dimensionless wall-layer thickness, $1-\alpha$, of 20% while those on the right correspond to a thickness of 10%. In all panels, the solid curve is associated with a reciprocal dimensionless wall drag, δ^2, of 0.001; the dashed curve corresponds to $\delta^2 = 0.01$. The dotted curve

shows the velocity profiles which arise in the absence of a wall layer. These velocity profiles are shown at three different axial positions on the sphere which are indicated by the vertical bar on the illustrations between adjacent panels.

As in the case without pellets, as δ^2 decreases, the pointwise velocity in the wall layer is diminished and approaches a uniform profile with a boundary layer or transitional region developing at the interface between the wall and lubrication layers. The smaller the value of δ^2, the greater the retardation of fluid in the wall layer. At the interface between the wall and lubrication layers, the fluid velocity has a greater deficit to overcome in the gap to achieve sphere velocity than it would at the corresponding radial position without a wall layer. Consequently, the shear stress in the lubrication layer is elevated and the *effective* clearance between the sphere and the tube wall can be regarded as diminished relative to a system without a wall layer. The increased shear stress in the lubrication layer is accompanied by an increase in the magnitude of the pressure gradient in the axial direction. Although the axial pressure distribution is qualitatively unchanged in the presence of a wall layer (see Özkaya 1986 and Skalak & Özkaya 1987 for pressure distributions of rigid spheres in smooth-walled tubes), the larger variations in pressure result in enhanced drag on the sphere and an increased total pressure drop across the sphere.

The enhanced resistance presented by the wall layer can be characterized by the ratio $\Delta p/Q_0$. Figure 5(*a*) shows, as a function of δ^2, the relative pressure drop, Δp, necessary to achieve the same volume flow as in a system having the same tube diameter and sphere-to-tube diameter ratio without a wall layer. Since the apparent viscosity, μ_{app}, is proportional to the resistance defined in this way, the ordinate in figure 5(*a*) also represents the ratio $\mu_{app}/(\mu_{app})_{rt}$ where $(\mu_{app})_{rt}$ is the apparent viscosity of the equivalent system in rigid smooth-walled tubes. The pressure drop, Δp, is determined by integrating the Reynolds equation given by (5.24) over the length of the sphere. The corresponding pressure drop, $(\Delta p)_{rt}$, for the equivalent system without a wall layer is obtained from the Reynolds equation derived for rigid spheres in rigid smooth-walled tubes (Tözeren & Skalak 1978). Thus the ratio of apparent viscosities shown in figure 5(*a*) is equivalent to the ratio of these pressure drops where Δp and $(\Delta p)_{rt}$ are both computed for a unit volume flow such that

$$\frac{\mu_{app}}{(\mu_{app})_{rt}} = \frac{\Delta p/Q_0}{(\Delta p)_{rt}/(Q_0)_{rt}}. \tag{6.1}$$

The normalized apparent viscosities shown in figure 5(*a*) correspond to the case when the sphere radius is 99.5% of the free-lumen radius. If a smaller sphere is considered, the effect of the wall layer on apparent viscosity is diminished.

Analogous to figure 3 for the case without pellets, figure 5(*b*) shows the volume flow, as a function of δ^2, for spheres flowing in a tube lined with a porous wall layer relative to a system under the equivalent driving pressure having the same tube diameter and sphere-to-tube diameter ratio without a wall layer. The volume flow, Q_0, was determined explicitly using (5.29). Taking a reference configuration attached to the tube wall, a similar expression was derived for $(Q_0)_{rt}$, the volume flow of a sphere flowing in a rigid smooth-walled tube. Both Q_0 and $(Q_0)_{rt}$ were scaled to correspond to a unit pressure drop in their respective systems in order to determine the normalized volume flow shown in figure 5. Normalizing the volume flow in this way provides a quantitative measure of the influence of the wall layer on the total material volume conduction through the tube.

Just as in the case without pellets, we anticipate a lower bound on the volume flow as that which would be obtained if the hydraulic resistivity in the wall layer were so large

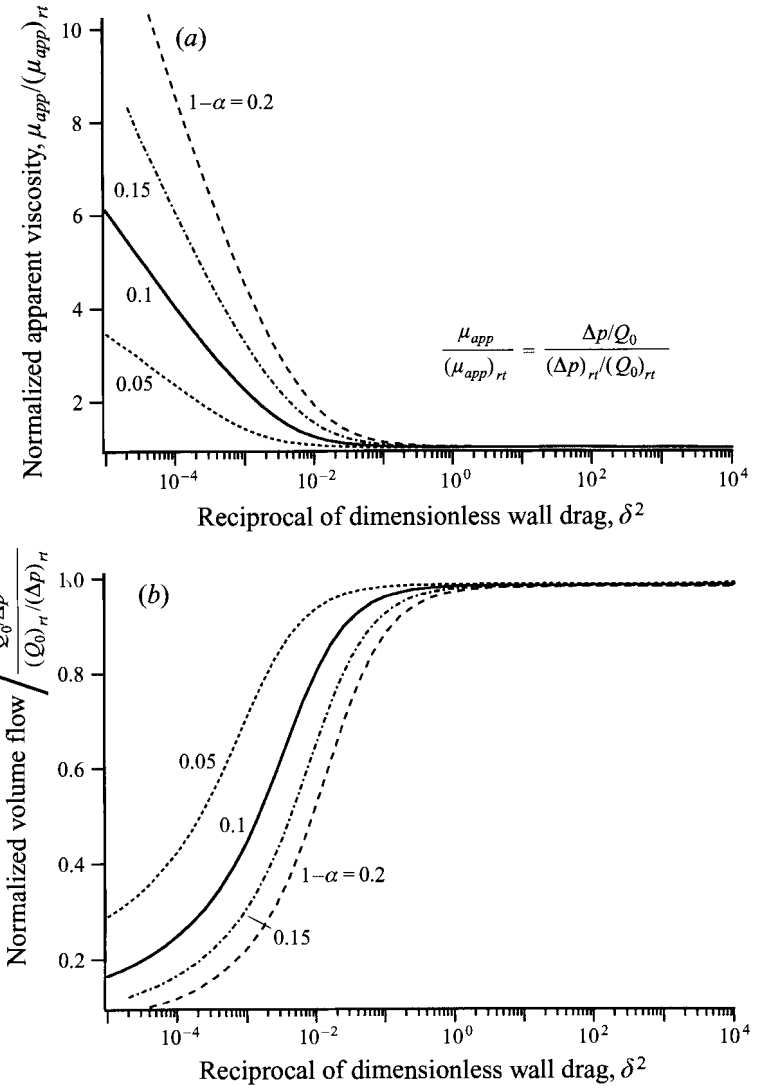

FIGURE 5. Normalized apparent viscosity (*a*) and volume flow (*b*) for a suspension of rigid spheres flowing in a tube lined with a porous wall layer as a function of the reciprocal dimensionless wall drag, δ^2, for four values of dimensionless wall-layer thickness, $1 - \alpha$ (5, 10, 15 and 20% of the tube radius). The apparent viscosity and total volume flow are normalized with respect to the corresponding values in the equivalent smooth-walled system having the same tube diameter and sphere-to-tube diameter ratio without a wall layer. The apparent viscosity is proportional to the resistance, $\Delta p/Q_0$, and therefore the ordinate in (*a*) also represents the relative driving pressure necessary to achieve the same volume flow as in the equivalent system without a wall layer. The relative volume flow per unit pressure drop in (*b*) expresses the total material volume conduction that would arise relative to the equivalent smooth-walled system under the same driving pressure. All parameters as in figure 4.

as to make it effectively impermeable. In particular, in the limit as δ^2 tends toward zero, the hydraulic resistivity becomes infinite and flow in the wall layer stops altogether. In this extreme, the effective radius of the tube is reduced, by the factor α, to the radius of the free lumen and the sphere-to-tube diameter ratio degenerates from $\alpha\lambda_0$ to λ_0. We may determine this lower bound by considering the ratio of the volume flow for

a sphere flowing in a smooth-walled tube having a diameter ratio of λ_0 to that which would arise with the same-sized sphere flowing under the same pressure drop in a tube having a diameter ratio of $\alpha\lambda_0$. For the wall-layer thicknesses considered in figure 5(*b*), we obtain the following lower-bound asymptotes: the dotted curve, corresponding to $1-\alpha = 5\%$ and $\lambda_0 = 99.5\%$, approaches the limit of approximately 0.192 from above, the solid curve ($1-\alpha = 10\%$) approaches 0.104, the dash-dotted curve ($1-\alpha = 15\%$) approaches 0.066, and the dashed curve ($1-\alpha = 20\%$) approaches 0.044. In the same manner we may determine the upper limits on the apparent viscosity. For the curves shown in figure 5(*a*), we obtain the upper-bound asymptotes of 5.2, 9.6, 15.3, and 22.5 for the dimensionless wall-layer thicknesses of 5, 10, 15, and 20%, respectively.

In addition to the apparent viscosity, another important rheological parameter is the hematocrit. Since the mean velocity of the fluid is always less than the sphere velocity (see figure 4), the volume fraction of pellets in the tube, referred to as tube hematocrit, H_T, will be less than the discharge hematocrit, H_D, which corresponds to the volume fraction of pellets in the suspension after it has been collected. Figure 4 illustrates the mechanism by which a wall layer causes a reduction in tube hematocrit relative to the equivalent system without a wall layer having the same discharge hematocrit. The diminished volume flow through the wall layer results in a greater disparity arising between the mean fluid velocity and the sphere velocity, producing a decreased tube hematocrit. For a fixed discharge hematocrit, the presence of a wall layer would therefore result in a decreased lineal density of spheres (number of spheres per unit length) relative to the equivalent system without a wall layer. It is easily shown that the ratio H_T/H_D is equal to the ratio of mean velocity to pellet velocity (Özkaya 1986). Since the dimensionless volume flow, Q_0, is defined relative to sphere velocity, if we divide by the dimensionless cross-sectional area, we find $H_T/H_D = 2Q_0$. For a given discharge hematocrit, the tube hematocrit in porous-walled tubes relative to smooth-walled tubes is therefore given by

$$\frac{H_T/H_D}{(H_T)_{rt}/(H_D)_{rt}} = \frac{Q_0}{(Q_0)_{rt}} \tag{6.2}$$

where $(H_T)_{rt}$ and $(H_D)_{rt}$ are, respectively, the tube and discharge hematocrits in smooth-walled tubes. Figure 6(*b*) reveals the influence of the wall layer on tube hematocrit by showing (6.2) as a function of δ^2 for several values of dimensionless wall-layer thickness, $1-\alpha$. According to (6.2), figure 6(*b*) also represents the volume flow through a tube lined with a porous wall layer relative to the volume flow which would arise in a system having the same sphere velocity, tube diameter, and sphere-to-tube diameter ratio without a wall layer. Figure 6(*a*) shows, as a function of δ^2, the relative pressure drop across a sphere needed to achieve the same sphere velocity as a system having the same tube diameter and sphere-to-tube diameter ratio without a wall layer. In order to determine the normalized driving pressure shown in figure 6(*a*), both Δp and $(\Delta p)_{rt}$ were non-dimensionalized in such a way as to correspond to a unit sphere velocity. The curves shown in figure 6 correspond to the case when the sphere radius is 99.5% of the free-lumen radius. If a smaller sphere is considered, the effect of the wall layer on tube hematocrit is enhanced while its effect on pressure drop is diminished.

Just as a lower bound on the normalized material volume conduction can be determined in the limit of zero flow in the wall layer, based on the same reasoning we can obtain lower-bound asymptotes on tube hematocrit for the curves in figure 6(*b*). For a sphere which is 99.5% of the free-lumen radius and dimensionless wall-layer thicknesses of 5, 10, 15, and 20%, the corresponding tube hematocrits can be reduced relative to smooth-walled tubes by at most the factors 0.962, 0.916, 0.865, and 0.809,

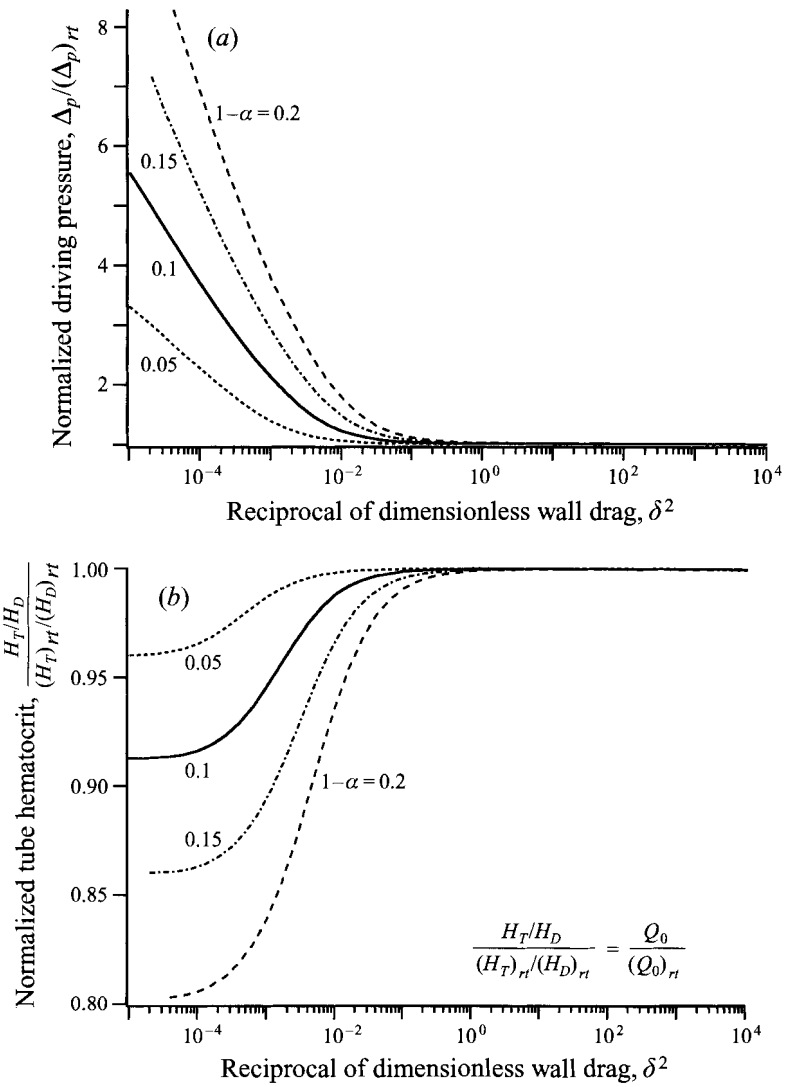

FIGURE 6. Normalized driving pressure (*a*) and tube hematocrit (*b*) for a suspension of rigid spheres flowing in a tube lined with a porous wall layer as a function of the reciprocal dimensionless wall drag, δ^2, for four values of dimensionless wall-layer thickness, $1-\alpha$ (5, 10, 15 and 20% of the tube radius). The pressure drop over the sphere and the tube hematocrit are normalized with respect to the corresponding values in the equivalent smooth-walled system having the same tube diameter and sphere-to-tube diameter ratio without a wall layer. In particular, (*a*) represents the pressure drop necessary to achieve a unit sphere velocity relative to the corresponding value in the equivalent smooth-walled system and (*b*) represents the tube hematocrit necessary to achieve a given discharge hematocrit relative to the corresponding value in the equivalent smooth-walled system. Since the ratio of tube to discharge hematocrit is twice the dimensionless volume flow, the ordinate in (*b*) also expresses the relative total volume flow that arises per unit sphere velocity. All parameters as in figure 4.

respectively. An upper bound on the driving pressure per unit sphere velocity can also be determined. The curves in figure 5(*b*), corresponding to the dimensionless wall-layer thicknesses of 5, 10, 15, and 20% asymptote, respectively, to 5.01, 8.83, 13.21, and 18.22 from below.

7. Application to capillary blood flow

The results of the preceding analysis have interesting implications for the rheology of blood in the microcirculation. In §1 we identified the glycocalyx, presented on the luminal surface of the capillary endothelial cells, as a structure which might exhibit similar behaviour to a biphasic wall layer. Although only limited data are available on material properties pertaining to the glycocalyx, a great deal is known about one of its possible constituents. In particular, the permeability and porosity of fibrinogen gels have been measured *in vitro* by Blombäck & Okada (1982) and Blombäck *et al.* (1989). Estimates of the elastic modulus of these gels were reported from measurements made by King *et al.* (1988) and Procyk & King (1990).

Fibrin gel structures have been reported as containing more than 99% water (Blombäck *et al.* 1989). This corresponds to a solid volume fraction, ϕ^s, of around 0.01 for this material. Solid volume fractions below 0.05 are not uncommon in biological materials. For example, Levick (1987) reported glycosaminoglycan volume fractions of a variety of interstitial tissues as ranging from 3.25×10^{-4} (vitreous body) to 0.03 (femoral head cartilage). A similar range was reported for proteoglycan volume fractions. Interstitial materials containing low collagen-fibril volume fractions were reported as having high void volumes. Since the glycocalyx is composed primarily of glycoproteins and proteoglycans, and is unlikely to contain collagen fibrils, we assume its porosity to be consistent with the value reported by Blombäck *et al.* (1989) for fibrinogen gels and take $\phi^f = 0.99$. Assuming that plasma proteins are not likely to be excluded from the glycocalyx, we take the viscosity of the fluid phase in the wall layer to be nearly equal to that of the plasma in the free lumen (i.e. $\mu^f = \mu^l$) and thus, $\eta = 0.98$. All of the figures presented here correspond to $\phi^f = 0.99$ and $\eta = 0.98$.

Blombäck & Okada (1982) and Blombäck *et al.* (1989) studied the structure of fibrin gels by confocal laser microscopy and conducted liquid permeation studies to measure the permeability of the gels as a function of clotting time and fibrin concentration. They computed Darcy's coefficient, K_D, by measuring the volume flow, $\dot{Q}$, of a liquid through a gel column of height L, and cross-sectional area A_c, under an imposed pressure differential, Δp. For a fluid having viscosity μ, they computed Darcy's constant according to

$$K_D = \frac{\dot{Q} L \mu}{A_c \Delta p}. \tag{7.1}$$

By comparing Darcy's law for fluid flow in a porous medium with the constitutive equations from mixture theory which we have employed, we obtain a relationship between the permeability or hydraulic conductivity, k, and Darcy's constant, K_D, given by $k = K_D \phi^f / \mu^f$. Since the permeability has been shown to be inversely proportional to the hydraulic resistivity, K, according to $k = (\phi^f)^2 / K$ (Lai & Mow 1980), we obtain the relationship between Darcy's constant and δ^2 given by

$$K_D = \phi^f R^2 \delta^2 \tag{7.2}$$

where R is the characteristic radius of the tube. From their measurements of Darcy's constant, Blombäck & Okada (1982) found K_D in fibrin gels to range between 10^{-10} and 10^{-8} cm^2. For a fibrin gel having a fluid volume fraction of 0.99 and a fluid phase corresponding to blood plasma with a viscosity of 0.012 dyn s cm^{-2}, the hydraulic conductivity ranges between 8.3×10^{-9} and 8.3×10^{-7} cm^4(dyn s)$^{-1}$. For a characteristic radius, R, corresponding to a 4 μm capillary, the reciprocal of the dimensionless wall drag ranges between 6×10^{-4} and 6×10^{-2}. According to Blombäck

& Okada (1982), Darcy's constant (and thus δ^2) was seen to decrease exponentially with increasing fibrin concentration, increasing ionic strength, and increasing pH of the gel.

Levick (1987) reported values of hydraulic conductivity, k, for various tissues and interstitial materials. For the sake of comparison with the range of permeabilities we will be using for the endothelial-cell glycocalyx, we consider some of the materials which Levick reported. In particular, he included two values for the hydraulic conductivity of the mesentery as being 1.9×10^{-10} and 3.1×10^{-11} cm^4(dyn s)$^{-1}$. The hydraulic conductivity associated with the vitreous body, which was closest to the range corresponding to fibrinogen gels, was reported as being between 2.1 and 4.2×10^{-9} cm^4(dyn s)$^{-1}$. By comparison, the permeability of the path across the capillary wall is between one and two orders of magnitude lower than the permeability of the mesentery (Levick 1987) which in turn is between one and three orders of magnitude lower than the permeability of fibrinogen gels (Blombäck & Okada 1982; Blombäck *et al.* 1989).

Despite the relatively high hydraulic conductivity of fibrinogen gels, a material such as this can significantly retard flow in porous-walled tubes. According to figure 3, for $\delta^2 = 0.001$ and a wall-layer thickness which is 10% of the tube radius (solid curve), we find the volume flow is diminished in pellet-free plasma to 73% of the Poiseuille-flow value in a rigid smooth-walled tube under the same pressure drop. Doubling the thickness of the wall layer reduces the volume flow to 46% of the Poiseuille-flow value. If a rigid sphere is introduced that is 99.5% of the free-lumen radius, according to figure 5(*b*), for $\delta^2 = 0.001$ and a wall-layer thickness which is 10% of the tube radius (solid curve), the total volume flow is diminished to 37% of the value in the equivalent system under the same pressure drop and having the same tube diameter and sphere-to-tube diameter ratio without a wall layer. Doubling the wall-layer thickness reduces the total volume flow to 18% of the value in smooth-walled tubes. We summarize these results for the case with spheres in figure 7 by plotting the apparent viscosity and tube hematocrit, relative to smooth-walled tubes, as a function of the dimensionless wall-layer thickness for two values of δ^2. In both (*a*) and (*b*), the solid curve corresponds to $\delta^2 = 0.001$ and the dashed curve corresponds to $\delta^2 = 0.01$. The solid curve, therefore, lies near the lower bound on the permeability of fibrinogen gels while the dashed curve lies near the upper bound.

The most pronounced effect of the porous wall layer is the marked increase in apparent viscosity relative to spheres flowing in smooth-walled tubes. In the range of permeabilities associated with fibrinogen gels, the presence of a 15% wall-layer thickness results in a two- to four-fold increase in apparent viscosity when a sphere, which is 99.5% of the free-lumen radius, is flowing in the free lumen. For smaller spheres, the increased resistance is less pronounced. If a sphere which is only 80% of the free-lumen radius is considered, the apparent viscosity is elevated only 1.5 to 2 times over the value in smooth-walled tubes having a sphere-to-tube diameter ratio of 68% ($\alpha\lambda_0 = 0.85 \times 0.8$). Despite the model's inherently crude geometric approximations of capillary blood flow, for closely fitting spheres in the free lumen the increase in apparent viscosity which the model predicts is consistent with the four-fold increase Pries *et al.* (1994) predicted in 10 μm capillaries.

On the other hand, owing to the simplified axisymmetric geometry considered here, the model can have only a modest effect on capillary tube hematocrit. In the range of permeabilities associated with fibrinogen gels, the presence of a wall layer which is 15% of the tube radius results in a reduction in tube hematocrit of only 4 to 12% for spheres which are 99.5% of the free-lumen radius. If a smaller sphere is considered,

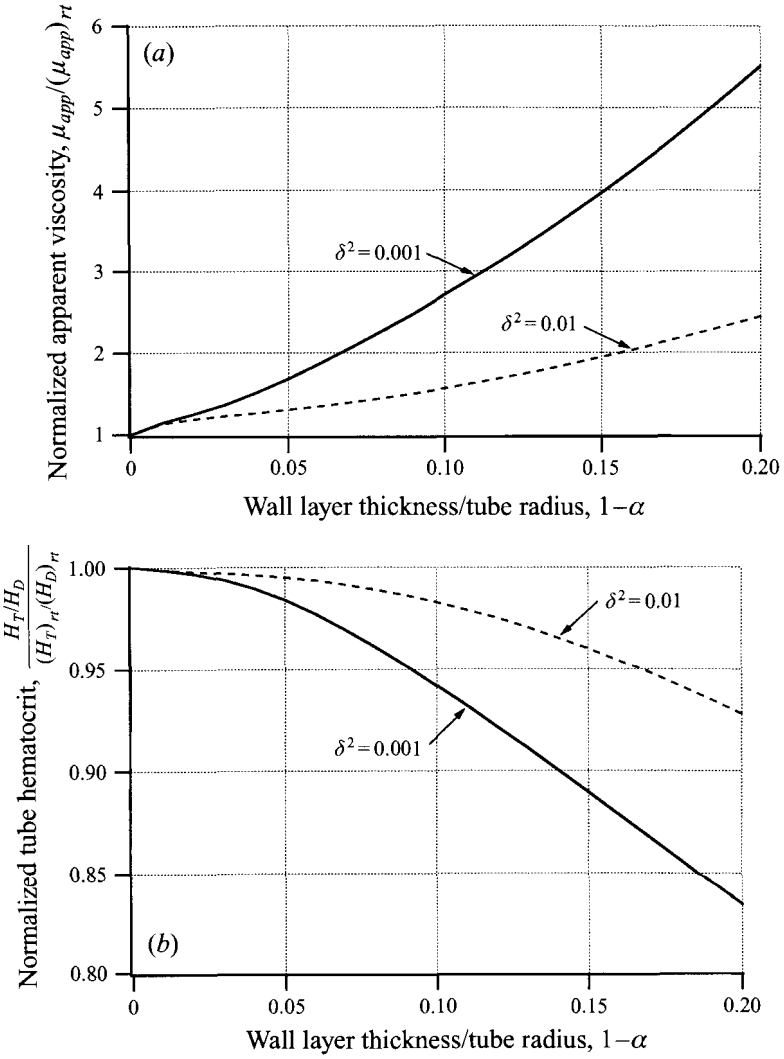

FIGURE 7. Normalized apparent viscosity (*a*) and tube hematocrit (*b*) for a suspension of rigid spheres flowing in a tube lined with a porous wall layer as a function of the dimensionless wall-layer thickness corresponding to two values of δ^2. The apparent viscosity and tube hematocrit are normalized with respect to the corresponding values in the equivalent smooth-walled system having the same tube diameter and sphere-to-tube diameter ratio without a wall layer. The smaller value of δ^2 (solid curves) is near the lower bound on the permeability of fibrinogen gels and the larger value (dashed curves) is near the upper bound. All parameters as in figure 4.

which for example is 80% of the free-lumen radius, a 9 to 18% reduction in tube hematocrit is observed relative to an equivalent smooth-walled system.

Desjardins & Duling (1990) conducted *in vivo* microperfusions in capillaries with enzymes which digested macromolecules in the glycocalyx to study the effect this structure might have on capillary tube hematocrit. In particular, treatment with heparinase resulted in at least a two-fold increase in tube hematocrit. They proposed that the glycocalyx might act to retard plasma and thereby increase the disparity between the red-cell and mean blood velocities. Heparinase treatment presumably cleaved the glycocalyx and removed the extracellular matrix which thereby reduced

or removed the retarded plasma layer. This hypothesis is as much dependent upon the shapes which red cells can assume in capillaries as it is upon the size and structure of the wall layer. This analysis can only begin to address the second of these two factors. For even in the most extreme case, if flow were to stop altogether in the wall layer, the disparity between mean blood velocity and sphere velocity remains small for clearances less than 20% (observe that the total change in relative tube hematocrit for the dashed curve in figure 6(*b*) is less than 20%). It is noteworthy that even for a relatively permeable material such as fibrinogen, the diminution in tube hematocrit predicted by the model for a wall layer which is 20% of the tube radius represents 40 to 90% of the maximum possible reduction for the axisymmetric configuration considered here. It is conceivable that for sufficiently asymmetric cell shapes, which are associated with inherently lower ratios of mean blood velocity to red-cell velocity, the presence of a wall layer could have a greater influence on capillary tube hematocrit than it does with the simple axisymmetric pellets that this analysis addresses. Thus, the modest reduction in tube hematocrit predicted by the model for small clearances is fundamentally limited by the geometric constraints imposed on the system.

Aside from complicated geometries, other factors not considered in this analysis might play an important role in influencing the apparent viscosity resulting from a porous wall layer. For one thing, we do not expect the approximation of a linearly elastic solid phase in the wall layer to accurately approximate the elastic behaviour of the glycocalyx, especially in the light of the large radial deformations that the glycocalyx might experience on the passing of very tightly fitting red cells through the smallest capillaries. In consideration of the elastic properties of fibrinogen gels (King *et al.* 1988; Procyk & King 1990), for capillary diameters smaller than red-cell diameters (below 8 μm), we anticipate considerable radial deformation of the glycocalyx resulting in significant reorganization of the solid matrix. We have therefore limited our attention to pellets which were constrained to maximum diameters strictly less than the diameter of the free lumen. It should be pointed out, however, that, under physiological flow conditions, the solid-phase displacements shown in figure 2(*b*) experience axial strains on the order of 50% for a wall layer hydrated in plasma having the elastic properties and permeability of fibrinogen gels. Such large deformations, while not unusual for biological materials, certainly lie outside the range of the infinitesimal-strain theory used here. Furthermore, the permeability, and thus the hydraulic resistivity, of similar biological materials tends to be quite sensitive to the normal strain (Mow *et al.* 1980; Lai & Mow 1980). Therefore, significant variations in material properties might accompany large deformations of the glycocalyx. In this preliminary analysis, we have limited our attention to a biphasic mixture. The red cell and the glycocalyx, however, are both known to be electronegative. A triphasic mixture model could incorporate an ionic phase into an analysis which studies the effect of charge interactions within the glycocalyx. From a purely mechanical point of view, this charge interaction might result in a repulsive force strong enough to induce radial deformations of the glycocalyx and/or red cell. This in turn could increase the clearance between the red cell and wall layer and reduce the drag on the cell. A larger lubrication layer (accompanied by a diminished wall-layer thickness) might be offset to some extent by the increased drag in the wall layer which could accompany radial deformation of the glycocalyx. Finally, in the analysis presented here, only viscous forces in the fluid and drag-interaction forces in the wall layer must be overcome in order to drive the pellets through the tube. In fact, the driving pressure necessary to force tightly fitting red cells along capillaries must additionally overcome the restoring forces both in the red-cell membrane and

imposed by the solid matrix comprising the glycocalyx on the passing cell. Models of red-cell deformation under pressure-driven flow in cylindrical tubes abound in the literature (Lighthill 1968; Barnard *et al.* 1968; Skalak & Özkaya 1987; Skalak *et al.* 1989; Secomb *et al.* 1986; Secomb 1991, 1995). These models all conclude that the stiffness of the red-cell membrane and the deformability of that structure are of fundamental importance in the resistance to blood flow in the microcirculation. Thus, a truly descriptive model of capillary rheology must incorporate the additional fluid–structure interactions which arise in the presence of a deformable pellet. Furthermore, a realistic model of the red cell might also include the erythrocyte glycocalyx modelled in the same manner in which it was handled here for the endothelial cell. Geometric variation, surface–charge interactions, strain-dependent material properties of the glycocalyx, and large deformations of both the glycocalyx and red cell are likely to play a major role in the rheological behaviour of the system as a whole. A finite-deformation theory for the wall layer which includes this additional physics would result in a complex system of coupled nonlinear partial-differential equations which are analytically intractable and require numerical solution. It is hoped that the model presented here, while remaining simple enough to admit closed-form solutions, still contains sufficient detail to elucidate some of the salient aspects associated with hydroelastic interactions within the wall layer arising from a pressure-driven axial flow.

The authors gratefully acknowledge Dr Richard Skalak for useful discussions regarding various theoretical aspects of the model. We would also like to thank Dr Hans Vink for his participation in discussions relating to various experimental findings. Support for this work was provided by NIH grants HL-07284, HL-12792, HL-54136, and HL-49146.

REFERENCES

BARNARD, A. C. L., LOPEZ, L. & HELLUMS, J. D. 1968 Basic theory of blood flow in capillaries. *Microvasc. Res.* **1**, 23–34.

BEAVERS, G. S. & JOSEPH, D. D. 1967 Boundary conditions at a naturally permeable wall. *J. Fluid Mech.* **30**, 197–207.

BLOMBÄCK, B., CARLSSON, K., HESSEL, B., LILJEBORG, A., PROCYK, R. & ÅSLUND, N. 1989 Native fibrin gel networks observed by 3D microscopy, permeation and turbidity. *Biochim. Biophys. Acta* **997**, 96–110.

BLOMBÄCK, B. & OKADA, M. 1982 Fibrin gel structure and clotting time. *Thromb. Res.* **25**, 51–70.

CHIEN, S., USAMI, S., TAYLOR, H. M., LUNDBERG, J. L. & GREGERSEN, M. I. 1966 Effects of hematocrit and plasma proteins on human blood rheology at low shear rates. *J. Appl. Physiol.* **21**, 81–87.

COPLEY, A. L. 1974 Hemorheological aspects of the endothelium-plasma interface. *Microvasc. Res.* **8**, 192–212.

DESJARDINS, C. & DULING, B. R. 1990 Heparinase treatment suggests a role for the endothelial cell glycocalyx in regulation of capillary hematocrit. *Am. J. Physiol.* **258**, H647–H654.

FITZ-GERALD, J. M. 1969 Mechanics of red-cell motion through very narrow capillaries. *Proc. R. Soc. Lond.* B **174**, 193–227.

GRETZ, J. E. 1995 The role of capillary anatomical and functional dimensions in capillary tube hematocrit variability. PhD thesis, University of Virginia, Charlottesville, VA.

HOU, J. S., HOLMES, M. H., LAI, W. M. & MOW, V. C. 1989 Boundary conditions at the cartilage-synovial fluid interface for joint lubrication and theoretical verifications. *J. Biomech. Engng* **111**, 78–87.

HOU, J. S., HOLMES, M. H., LAI, W. M. & MOW, V. C. 1990 Squeeze film lubrication for articular cartilage with synovial fluid. In *Biomechanics of Diarthrodial Joints* (ed. V. C. Mow, A. Ratcliffe & S. L-Y. Woo), pp. 347–367. Springer.

KING, K., PROCYK, R., CHIEN, S., BLOMBÄCK, B. & COPLEY, A. L. 1988 The effect of factor XIII and fibronectin on the viscoelasticity of fibrinogen surface layers. *Thromb. Res.* **49**, 139–144.

KLITZMAN, B. & DULING, B. R. 1979 Microvascular hematocrit and red cell flow in resting and contracting striated muscle. *Am. J. Physiol.* **237**, H481–H490.

KRINDEL, P. & SILBERBERG, A. 1979 Flow through gel-walled tubes. *J. Colloid Interface Sci.* **71**, 39–50.

LAHAV, J., ELIEZER, N. & SILBERBERG, A. 1973 Gel-walled cylindrical channels as models for the microcirculation: Dynamics of flow. *Biorheology* **10**, 595–604.

LAI, W. M. & MOW, V. C. 1980 Drag-induced compression of articular cartilage during a permeation experiment. *Biorheology* **17**, 111–123.

LEVICK, J. R. 1987 Flow through interstitium and other fibrous matrices. *Q. J. Exp. Physiol.* **72**, 409–438.

LIGHTHILL, M. J. 1968 Pressure-forcing of tightly fitting pellets along fluid-filled tubes. *J. Fluid Mech.* **34**, 113–143.

MOW, V. C., KUEI, S. C., LAI, W. M. & ARMSTRONG, C. G. 1980 Biphasic creep and stress relaxation of articular cartilage in compression: Theory and experiments. *J. Biomech. Engng* **102**, 73–84.

ÖZKAYA, N. 1986 Viscous flow of particles in tubes: Lubrication theory and finite element models. PhD thesis, Columbia University, New York, NY.

PRIES, A. R., NEUHAUS, D. & GAEHTGENS, P. 1992 Blood viscosity in tube flow: dependence on diameter. *Am. J. Physiol.* **263**, H1770–H1778.

PRIES, A. R., SECOMB, T. W., GAEHTGENS, P. & GROSS, J. F. 1990 Blood flow in microvascular networks: experiments and simulation. *Circ. Res.* **67**, 826–834.

PRIES, A. R., SECOMB, T. W., GEßNER, T., SPERANDIO, M. B., GROSS, J. F. & GAEHTGENS, P. 1994 Resistance to blood flow in microvessels in vivo. *Circ. Res.* **75**, 904–915.

PROCYK, R. & KING, K. 1990 The elastic modulus of fibrin clots and fibrinogen gels: the effect of fibronectin and dithiothreitol. *Biopolymers* **29**, 559–565.

SECOMB, T. W. 1991 Red blood cell mechanics and capillary blood rheology. *Cell Biophys.* **18**, 231–251.

SECOMB, T. W. 1995 Mechanics of blood flow in the microcirculation. In *Biological Fluid Dynamics* (ed. C. P. Ellington & T. J. Pedley), pp. 305–321. Company of Biologists, Cambridge.

SECOMB, T. W., SKALAK, R., ÖZKAYA, N. & GROSS, J. F. 1986 Flow of axisymmetric red blood cells in narrow capillaries. *J. Fluid Mech.* **163**, 405–423.

SKALAK, R. & ÖZKAYA, N. 1987 Models of erythrocyte and leukocyte flow in capillaries. In *Physiological Fluid Dynamics II* (ed. L. S. Srinath & M. Singh), pp. 1–10. Tata McGraw-Hill, New Delhi.

SKALAK, R., ÖZKAYA, N. & SKALAK, T. C. 1989 Biofluid mechanics. *Ann. Rev. Fluid Mech.* **21**, 167–204.

TÖZEREN, H. & SKALAK, R. 1978 The steady flow of closely fitting incompressible elastic spheres in a tube. *J. Fluid Mech.* **87**, 1–16.

TRUESDELL, C. & TOUPIN, R. 1960 The classical field theories. In *Handbuch der Physik* (ed. S. Flügge), pp. 226–793. Springer.

WANG, W. & PARKER, K. H. 1995 The effect of deformable porous surface layers on the motion of a sphere in a narrow cylindrical tube. *J. Fluid Mech.* **283**, 287–305.

WANG, H. & SKALAK, R. 1969 Viscous flow in a cylindrical tube containing a line of spherical particles. *J. Fluid Mech.* **38**, 75–96.